Applied Magnetic Resonance (2023) 54:895–904
https://doi.org/10.1007/s00723-023-01580-5

Applied
Magnetic Resonance

ORIGINAL PAPER

MRI of Inanimate Objects Using Fluorine-Containing Liquid

Nikolay V. Anisimov[1] · Lev L. Gervits[2] · Arina A. Tarasova[3] · Ivan A. Usanov[3] · Yury A. Pirogov[3]

Received: 5 June 2023 / Revised: 20 July 2023 / Accepted: 22 July 2023 /
Published online: 28 July 2023

Abstract

The paper shows the possibilities of using a fluorine-containing liquid—the so-called dry water for the MRI of inanimate objects using the signal void imaging method. Examples of visualization of objects that cannot be immersed in ordinary water and other liquid media that can dissolve or spoil the object under study are presented. The possibilities of visualization of a radio engineering product immersed in dry water during its operation are shown. Namely, the coil, which itself is involved in the scanning process, is used to receive and/or transmit RF power. It is shown that the images of the medium surrounding the coil obtained in this case make it possible to construct sensitivity maps and B_1 maps of this coil. The issues of optimization of scanning parameters based on information about the ^{19}F NMR spectrum and measurements of relaxation times for a given liquid are discussed.

✉ Nikolay V. Anisimov
anisimovnv@mail.ru

Lev L. Gervits
gervits@ineos.ac.ru

Arina A. Tarasova
arina.tarasova99@mail.ru

Ivan A. Usanov
usanov.ia17@physics.msu.ru

Yury A. Pirogov
yupi937@gmail.com

[1] Faculty of Fundamental Medicine, Lomonosov Moscow State University, 119991 Moscow, Russian Federation

[2] Nesmeyanov Institute of Organoelement Compounds of the Russian Academy of Sciences, 119334 Moscow, Russian Federation

[3] Faculty of Physics, Lomonosov Moscow State University, 119991 Moscow, Russian Federation

1 Introduction/Purpose

Magnetic resonance imaging (MRI) is usually associated with medical diagnostics [1]. However, this method is also successfully used for non-medical technological applications—MR microscopy [2], food analysis [3], etc. MRI can also be used to visualize inanimate objects, from which it is difficult to obtain an acceptable NMR signal, for example, due to the lack of hydrogen in the material from which it is made. In this case, one can apply our method, which in this work is designated as signal void imaging. The method involves immersing an object in a medium with a substance acting as a contrast agent. This substance gives a strong background signal on the MR image, and the object is detected by the loss of the signal in this background [4, 5]. Structuring the fragmented areas of the signal loss allows building a three-dimensional image of the object. If, before volumetric reconstruction, simple manipulations with the data matrix are carried out—its individual fragments are zeroed out, then as a result of reconstruction, invisible parts of the object can be displayed or imagine how it would look after processing with a special tool–see Appendix 1.

For a wide range of objects, ordinary water can be used as a contrast agent. We have successfully used the signal void imaging method for volumetric imaging of glass, ceramics, rubber, bones, etc. [5], as well as metallic non-ferromagnetic objects—see Appendix 2.

In addition to protons, the signal void imaging method can also detect other nuclei. For example, sodium ^{23}Na, for which it is enough to add table salt to the water—see Appendix 3.

The problem with using water in the signal void imaging method is that some objects cannot be immersed in it due to irreversible changes after extraction. For example, paper products, food products. In this case, gas can be used. To achieve the highest signal-to-noise ratio (*SNR*), a hyperpolarized inert gas [6] can be used, but acceptable results are also obtained for fluorinated gases. We successfully used octafluorocyclobutane gas (OFCB, C_4F_8), which was previously used for ^{19}F MRI of human lungs [7]. With its help, three-dimensional images of a paper book and flour product were obtained [8].

The sensitivity of ^{19}F MRI for the detection of OFCB gas signal is two orders of magnitude lower than that of ^{1}H MRI for the detection of water signal. This makes it difficult to apply the signal void imaging method using gas, especially in a low field. To achieve an acceptable *SNR*, it is necessary to increase the voxel size, which reduces image detail, and/or carry out multiple signal accumulation, which, accordingly, increases the scanning time. The inconvenience of using gases in MRI is the need for good sealing of the container into which the object under study is immersed, after which it is difficult to re-position or fix it.

In search of a more suitable substance for the signal void imaging method, we turned our attention to a fluorine-containing liquid—the so-called dry water [9, 10]. It is used as an electronics coolant liquid and fire protection fluid. Visually, the liquid is similar to pure water but is not a solvent. The substance in its original form is non-toxic, has an extremely low solubility in water. It does not destroy

paper documents and works of art. It is dielectric ($\varepsilon = 2.3$), does not conduct electricity, therefore, it does not affect working electronics.

It can be assumed that many other objects after immersion in dry water and subsequent extraction will remain intact. At the same time, due to its low surface tension and low viscosity, it wets a variety of surfaces well and penetrates into the pores of an object immersed in it. These properties are essential for a contrast agent in the signal void imaging method. Of the various modifications of this product, we are interested in the product *Novec 1230* [9]. Its molecule is $CF_3CF_2C(O)CF(CF_3)_2$. It contains 12 fluorine atoms—the largest number of fluorine atoms among other similar products. Therefore, it can be expected that such a substance should give the strongest signal when it is detected by NMR methods.

The NMR signal S is proportional to the product of the molar receptivity $R = \gamma^3 I(I+1)$, where γ is the gyromagnetic ratio and I is the spin of the nucleus, and the concentration C of nuclei per unit volume. The value of C is proportional to $\rho N/M$, where ρ is the density, M is the molecular weight, N is the number of resonant nuclei in the molecule. Denoting the values of these quantities for fluorine nuclei in dry water and protons in ordinary water by indices F and H, we have $R_F/R_H = 0.83$, $\rho_F/\rho_H = 1.72/1.0$, $M_F/M_H = 316/18$, $N_F/N_H = 12/2$. According to these data, $S_F/S_H = 0.49$.

However, the difference in *SNR* for dry and ordinary water is somewhat greater than 0.49 due to the difference in the width of the NMR spectra. The width of the detected spectrum ΔF determines the sampling rate BW, which, in turn, determines the receiver bandwidth and the thermal noise that is proportional to $BW^{1/2}$. To avoid chemical shift artifacts, the value of BW must be greater than $\Delta F \cdot N$, where N is the number of digitized points in the direction of frequency coding [1]. The proton spectrum of ordinary water is a singlet, and therefore extremely narrow. In the ^{19}F NMR spectrum of dry water, according to the formula, there should be at least 4 peaks with different chemical shifts—from $(CF_3)_2$, CF_3, CF_2 and CF groups, the range of which can exceed 120 ppm [11]. For our field of 0.5 Tesla, this corresponds to a ΔF value greater than 2 kHz, and since N is usually set from several tens, the value of BW should be tens of kHz.

The aim of the work was to test dry water as a contrast agent for the visualization of inanimate objects that do not give an NMR signal using the signal void imaging method. To do this, it was supposed to obtain an NMR spectrum, determine the relaxation times, and, based on these data, optimize the scanning parameters. As a result of MR scanning, it was supposed to obtain ^{19}F MR images of objects that cannot be immersed in ordinary water—pieces of soluble sugar, dried scorpion, as well as a multi-turn loop coil, including the situation when it works as a receiving and/or transmitting coil.

2 Materials and Methods

2.1 Hardware and Software

The experiments were carried out on a 0.5 T scanner *Tomikon S50* (*Bruker*, Ettlingen, Germany) equipped with a superconducting magnet (*Magnex*, Oxford, UK)

with a bore diameter of 60 cm, a 2-kW *LPPA*-2120 RF transmitter (*Dressler*, Stolberg, Germany), and an *S*630 gradient system with a maximum gradient strength of 16.7 mT/m and the rise time of 0.5 ms. Scanning control and data preprocessing were performed by embedded software *XWinNMR* v.1 and *ParaVision* v.1. Subsequent data processing, including *SNR* calculation and volumetric reconstructions, was performed using the *ImageJ* software package [12]. Additional details, including those related to the detection of nuclei other than protons and data treatment, are presented in [7, 8].

2.2 Coils

Three coils of different types were used in the experiments. We will denote them as CI, CII, and CIII. The first two (CI and CII) are proprietary saddle coils (part numbers T5973 and T3402) with inner diameters of 18 cm and 60 cm. CI is a receive-only quadrature coil. Usually, it is used for ^{1}H MRI studies (21.1 MHz) of human extremities, but in this work, it was used to detect fluorine signals (19.8 MHz) from dry water when the objects under study were immersed in it. The second coil (CII) built into the bore of the magnet was used both as a receiver and as a transmitter. The third coil (CIII) is a 6-turn loop in the shape of an oval with dimensions of 10×8.5 cm^2, connected with a cable to a transmit/receive switch. It is non-resonant, but it was used as a transceiver, as well as a passive object of visualization. In the latter case, the field B_1 was excited, and then the response was received by coil CII. Coils CI and CII resonant—are part of the resonant circuits. The quality factors Q for two quadrature channels of the CI coil are 345 and 425. For a single channel CII coil, $Q=310$.

2.3 Objects

Pieces of soluble sugar were placed in a plastic bottle 5 cm in diameter and 10 cm high, and filled with dry water. MR scanning was performed with a resolution of $2\times2\times2$ mm^3.

A stuffed dried scorpion (*Heterometrus spinifer*) was purchased as a decorative product, intended for hanging on the wall in a glazen wooden frame. The scorpion was removed from the frame and placed in a plastic container. The container with the stuffed animal was filled with dry water. As a result of drying, the tissues and internal organs inside the chitin shell greatly decreased in volume, which was filled with air. When the stuffed animal was immersed in dry water, this liquid replaced the air. The presence of dried tissue fragments inside the body of a scorpion can cause variations in contrast on individual slices, but they should not appear on the 3D rendering, which is built along the outer border of the object. The stuffed animal was kept from floating up by a net of nylon fishing line 0.14 mm. MR scanning was performed with a resolution of $1\times1\times1$ mm^3.

The object of the study was also coil CIII. It was immersed in a plastic container filled with dry water. Its axis was oriented perpendicular to both the polarizing field B_0 and the axis of the coil CII, and hence the field B_1 that it could

generate. The CIII coil could work either in passive or active mode. In the first case, the field B_1 was excited, and the dry water signal was received by the CII coil. In the active mode, the CIII coil could work as a transceiver, or in conjunction with the CII coil, as a transmitter only, or only as a receiver. In the passive mode, it was possible to visualize the CIII coil using the signal void imaging method. In the active mode, one can visualize the distribution of dry water signal near it, which corresponds to its sensitivity map and/or B_1 map. MR scanning was performed with a resolution of $5 \times 5 \times 5$ mm^3.

The commercial product *Novec 1230* (3M company) in a volume of 1 L was used as dry water [9]. The same liquid was used repeatedly—after experiments with one of the objects, the liquid was poured into an empty vessel, and then the liquid from this vessel was used for experiments with the next object. There were minor fluid losses due to overflows and partial evaporation.

MR scanning was performed using the 3D gradient recalled echo method [1]. Since the size of the scanning area exceeded the size of the scanned object, there was no need spatially to limit the RF excitation area. Therefore, RF excitation was carried out with rectangular pulses and without applying a slice-coding gradient. For all experiments, we set TE = 7 ms, BW = 30.3 kHz. To optimize the scan parameters FA and TR, the relaxation times T_1 were measured by the inversion-recovery method. As 90° and 180° pulses, we used pulses with a duration of 0.65 ms and 1.3 ms, respectively. The ^{19}F NMR spectrum was preliminarily obtained, in which lines from $(CF_3)_2$, CF_3, CF_2, and CF groups were determined (Fig. 1). For them, the T_1 values were measured, which were 1.60 s, 1.62 s, 1.73 s, and 1.88 s, respectively. In addition, for the CF_3 group, the value of T_2 was measured by the spin echo method, and the value of T_2* was determined by measuring the spectral line half-width. It was determined: $T_2 = 0.28$ s, $T_2^* = 15$ ms.

To visualize sugar and scorpion, we set $TR = 50$ ms. A rectangular pulse with duration $P = 125$ μs provided FA equal to the Ernst angle [1]. With our parameters T_1 and TR, it is equal to 14 degrees. The number of signal accumulations in

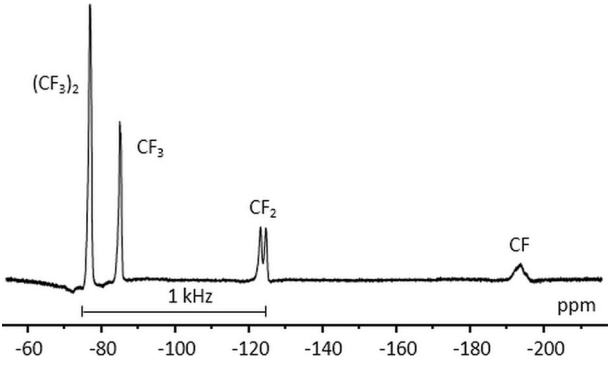

Fig. 1 ^{19}F NMR spectrum of dry water $CF_3CF_2C(O)CF(CF_3)_2$ at 0.5 Tesla (19.8 MHz). The scale is normalized by the chemical shift of trifluoroacetic acid

the first and second cases was 36 and 12, and the total scanning time was 1.5 and 5 h, respectively.

In experiments with coil CIII, it was supposed to obtain not only its image using the signal void imaging method in the passive mode but also its sensitivity and B_1 maps in active mode. It was supposed to build these 3D maps according to the contrast distribution for the space inside and outside the coil. To make the interpretation of these maps as simple as possible, we tried to set the scanning parameters so that the FA was as small as possible—at least not exceeding 45°. In this case, the spin response depends almost linearly on B_1. Since the field B_1 from the loop coil in the area of interest is non-uniform, we tried to provide a small FA (for definiteness, we have chosen FA = 34°) condition only for its center. To do this, an appropriate calibration was carried out for a small sample (1 cm^3), placing it in the center of the coil CIII. As a result, it was determined that the required value of FA was achieved at $P = 100$ μs.

A similar calibration was carried out for the CII coil. Since its dimensions are larger, the field B_1 turns out to be less than for coil CIII for the same input RF power, and the required FA was achieved at $P = 500$ μs. The difference would be even greater if coil CIII, like coil CII, were part of a resonant circuit. By the way, then the sensitivity of the coil CIII when receiving a signal would be higher. But the available sensitivity was enough. Therefore, experiments with the CIII coil were carried out without signal accumulation, and the scanning time for each of them was 10 min 14 s.

3 Results

Figure 2 shows ^{19}F MRI of objects immersed in dry water—sugar lumps, a scorpion, and a loop coil. They were obtained by the signal void imaging method. Individual slices and volumetric reconstructions are presented. For the loop coil, a minimum intensity projection (MinIP) is presented [1].

Figure 3A and B shows images of coil CIII immersed in dry water in two projections. They are presented in the form of *SNR* maps. The images were obtained when the B_1 field was excited by the CII coil, and the CIII coil was operating in the receive-only (RO) mode. For these maps, graphs of the dependence of the signal on the distance from the center of the coil in the diametrical and axial directions are presented—panels C and D, respectively. Similar images and graphs were obtained for other cases of using this coil in active mode—in the case when the CIII coil worked in the transmit-only mode (TO), and the CII coil was receiving, as well as in the case when the CIII coil worked both as a transmitter and as a receiver (TR). We present all the obtained graphs, but provide images only for the RO mode since the images for the other two modes visually differ little. It can only be noted that the image from mode TO has more noise.

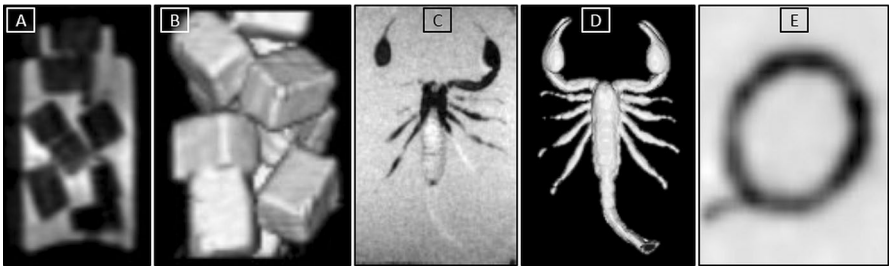

Fig. 2 ^{19}F MRI of objects immersed in dry water—sugar lumps **A**, **B**, scorpion **C**, **D**, loop coil **E**. A and C are individual slices; B and D—volumetric reconstructions—3D rendering. E–6-turn loop coil–MinIP reconstruction

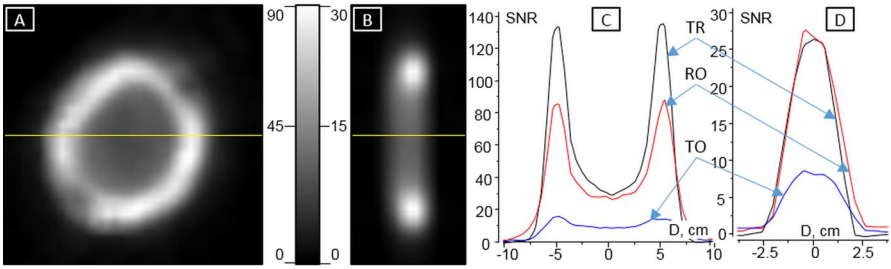

Fig. 3 A and B are *SNR* maps constructed from ^{19}F MR images in coronal and sagittal projections of the CIII coil immersed in dry water and at the same time operating in receive-only (RO) mode. C and D are graphs of the signal along the lines marked on the *SNR* maps for various operation modes of the coil CIII. Gray scale corresponds to *SNR* units. Abbreviations indicate: the distance from the center of the coil in centimeters (D, cm); coil operation options in active mode (see text): *RO* receive-only, *TO* transmit-only, *TR* transceiver

4 Discussion

Using a fluorine-containing liquid as a contrast agent, MR images of various objects were obtained. Images of satisfactory quality were obtained in an acceptable time, despite the relatively weak field B_0, as well as despite the fact that in a number of experiments a non-resonant coil was used when receiving a signal.

Images of a number of objects obtained by signal void imaging method can be obtained by X-ray computed tomography (CT), where there is no need to immerse the object in the imaging medium [13]. However, at the moment, for the ordinary user, the availability of CT is not much greater than that of MRI, due to administrative and other reasons. Therefore, it is useful to know about the possibilities of both methods. In particular, the fact that the coil sensitivity map can be obtained by MRI, but not by CT.

Usually, a coil sensitivity map is obtained by calculation, and the result is verified by measurements on a set of samples (phantoms) placed at separate points in

space. As a result, the experimentally obtained coil sensitivity map is discrete. Our method allows to obtain a continuous sensitivity map.

In addition to the loop coil, we have successfully carried out similar experiments with the solenoidal coil, preliminary results are presented in Appendix 4. We plan to carry out corresponding measurements for more complex coil configurations, in particular, quadrature coils. They contain current circuits for powering varicaps, pin diodes, and other active elements. Such elements and the coil itself are placed in an insulating housing, which can be visualized by proton MRI. We obtained the most informative proton images in the active mode of the coil—when the coil itself detects a signal from the surrounding hydrogen-containing materials, and at the same time, conductors are clearly identified against their background—see Appendix 5. Complementing these proton images with fluorine images of a coil immersed in dry water makes it possible not only to refine invisible structural details but also to construct sensitivity maps.

At first glance, the value of BW = 30.3 kHz set by us is insufficient to avoid chemical shift artifacts—with a spectral width ΔF of more than 2 kHz (see Fig. 1) and the number of digitized points N—up to 64, it should be 4 times larger. This artifact, indeed, was present, but it was hardly noticeable, since the main contribution to the signal—9/12 (75%) was from the $(CF_3)_2$ and CF_3 lines located at a distance of about 0.2 kHz. In principle, it is possible to suppress signals from peaks that are undesirable for detection by selective excitation methods or special data treatment [14].

It can be seen in Fig. 3, that the signal in the center of coils CII and CIII is the same in RO and TR modes. In these modes, signal is received by the same coil CIII, but the field B_1 is generated by different coils—CII and CIII, respectively. It follows that different coils give the same FA. Therefore, the same FA is also provided by CIII coil in the TO mode. Then, according to these graphs, one can compare the sensitivity of the CII and CIII coils—the sensitivity of a non-resonant coil CIII is 3.4 times higher than that of coil CII with a large quality factor.

This result can be explained by the fact that coils with different Q have different filling factors η. As is known, $\mathrm{SNR} \sim \eta \cdot Q^{1/2}$ [15]. The frame coil is a flat object. Therefore, a comparison of the filling factors of it and another coil makes sense only for the areas of the turns. The coil area is equal to $\pi D^2/4$, where D is the coil diameter. Then the SNR will be determined by the value of $D^{-2}Q^{1/2}$. Entering for the coils CII and CII the values D and Q with the corresponding indices, we have $D_{II}/D_{III} = 60/9$, $Q_{II}/Q_{III} = 310/1$. With this approach, the SNR for the CII coil will be 2.6 times less than for the CIII coil. Despite very rough estimates, we obtained a result not much different from the experimental one.

In the graph in Fig. 3, there is a noticeable difference in the proportions of the signals in the center and near the coils, especially for the RO and TO modes. Possibly, this is due to the fact that for the second mode near the turns, the condition of the smallness of FA is not satisfied. Indeed, a relatively small value for it FA = 34° was set for the center of the coil. But near the turns, it can increase several times. The increase can be estimated if we assume the validity of the reciprocity principle—a proportionality between the magnitude of the magnetic field generated by the current coil and the response of the coil to the action of an external field [1, 16]. This proportion can be estimated from the graph for the RO mode—the response to the action of a uniform field B_1, providing

FA = 34°. This graph shows that the difference in coil response for signals from voxels in the center and near the turns reaches 4.67. If we assume the same difference for the field B_1 generated by this coil, then near the turns FA can reach almost 160°. However, the interpretation of the principle of reciprocity should be approached very carefully. In our case, take into account that the field B_1 is homogeneous in the area of interest only in the RO mode, since a large coil generates it. In TO mode, field B_1 is generated by a small coil, and therefore is uniform only in a small area.

5 Conclusion

The signal void imaging technique can be used not only to visualize objects from which it is difficult to obtain an NMR signal directly but also to build coil sensitivity maps. Dry water is a convenient liquid for this technique. It gives a strong NMR signal. The liquid penetrates well into the cavities inside the object, evaporates slowly, and can be used repeatedly. Dry water is not-toxic, does not produce irreversible changes in the object in contact with it, and does not interfere with electronics. The problem is its high density, because of which it is necessary to keep objects immersed in it from floating up.

Supplementary Information The online version contains supplementary material available at https://doi.org/10.1007/s00723-023-01580-5.

Acknowledgements This research was supported by the Russian Foundation for Basic Research grants No. 19-29-10015 and Russian Scientific Foundation grant No. 21-75-10038, the Interdisciplinary Scientific and Educational Schools of Moscow University "Molecular Technologies of the Living Systems and Synthetic Biology" and "Photonic and quantum technologies. Digital medicine". Access to electronic scientific resources was provided by Nesmeyanov Institute of Organoelement Compounds of the Russian Academy of Sciences with the support of the Ministry of Science and Higher Education of the Russian Federation.

Author Contribution NVA and YuAP wrote the main manuscript text; LLG prepared Fig. 1; AAT prepared Fig. 2 and IAU prepared Fig. 3. All authors reviewed the manuscript.

Funding This research was supported by the Russian Foundation for Basic Research grants No. 19-29-10015 and Russian Scientific Foundation grant No. 21–75-10038.

Availability of Data and Materials The datasets generated during and/or analyzed during the current study are available from the corresponding author on reasonable request.

Declarations

Conflict of interest The authors declare no competing interests.

Ethical approval Not applicable.

References

1. E.M. Haacke, *Magnetic resonance imaging: physical principles and sequence design* (Wiley, New York, 1999), p.944

2. W. Kuhn, Angew. Chem. Int. Ed Engl. **29**, 1–112 (1990)
3. H. Ebrahimnejad, H. Ebrahimnejad, A. Salajegheh, H. Barghi, J. Biomed. Phys. Eng. **8**(1), 127–132 (2018)
4. N.V. Anisimov, Yu.A. Pirogov. Patent RU 2 308 025 C1 https://yandex.ru/patents/doc/RU2308025C1_20071010. Accessed 17 July 2023 (in Russian)
5. N.V. Anisimov, S.S. Batova, Yu.A. Pirogov, Magnetic resonance tomography: contrast control and interdisciplinary applications, (MAKS Press, Moscow, 2013), p. 244. (in Russian)
6. V.Z. Miloushev, K.R. Keshari, A. Holodny, Top Magn Reson Imaging. **25**(1), 31–37 (2016)
7. O.S. Pavlova, N.V. Anisimov, L.L. Gervits, M.V. Gulyaev, V.N. Semenova, Yu.A. Pirogov, V.Y. Panchenko, Magn. Reson. Med. **84**(4), 2111–2123 (2020)
8. N.V. Anisimov, O.S. Pavlova, A.A. Tarasova, I.A. Usanov, M.V. Gulyaev, Yu.A. Pirogov, Appl. Magn. Reson. **53**, 1575–1585 (2022)
9. Perfluoro(2-methyl-3-pentanone) https://en.wikipedia.org/wiki/Perfluoro(2-methyl-3-pentanone). Accessed 17 July 2023
10. Fire suppression—3M™ Novec™ 1230 Fire Protection Fluid https://www.3m.co.uk/3M/en_GB/novec-uk/applications/fire-suppression/. Accessed 17 July 2023
11. J.T. Gerig, Fluorine NMR, 1–35 https://www.biophysics.org/Portals/0/BPSAssets/Articles/gerig.pdf. Accessed 17 July 2023 (2001)
12. C.A. Schneider, W.S. Rasband, K.W. Eliceiri, Nat. Methods **9**(7), 671–675 (2012)
13. G. van Kaick, S. Delorme, Eur. Radiol. Suppl. **15**(Suppl 4), d74–d81 (2005)
14. M. Meissner, M. Reisert, T. Hugger, J. Hennig, D. von Elverfeldt, J. Leupold, Magn. Reson. Med. **73**, 2225–2233 (2015)
15. D.I. Hoult, P.C. Lauterbur, J. Magn. Reson. **34**, 425–433 (1979)
16. A.J. Ilott, A. Jerschow https://doi.org/10.48550/arXiv.1806.01390. Accessed 17 July 2023 (2018)